Journal of Electrical Engineering, Vol. 75, No. 4, 2024, pp. 268-274

sciendo

PAPERS

Comparative analysis of surface layer functionality in STM and AFM probes: Effects of coating on emission characteristics

Alexandr Knápek[1, 2, *], Mohammad M. Allaham[1, 3], Zuzana Košelová[1, 2], Daniel Burda[1,2], Jáchym Podstránský[1], Marwan S. Mousa[4], Dinara Sobola[1, 5]

Abstract: This study compares different types of scanning probe microscopy (SPM) probes according to the function of the surface layer at the tip apex. Three main types of SPM probes were analyzed: scanning tunneling microscopy (STM) tungsten probes, conductive atomic force microscopy (AFM) probes, and non-conductive AFM probes. The tungsten STM probes were coated with a graphite layer to simulate the effects of carbonization. The tested AFM probes were specifically NenoProbe conductive AFM probes (platinum-coated tip) and Akiyama non-conductive AFM probes coated with gold. The gold coating is intended to improve surface conductivity and help achieve a homogeneous, oxidation-resistant surface. The three samples were measured in a field emission microscope to study their current-voltage characteristics. The obtained current-voltage characteristics were tested and analyzed by the Forbes field emission orthodoxy test, providing the field emission parameters that correlate with the state of the scanning probe tip. In this study, the most important parameter is the formal emission area parameter, which indicates the formal tunneling current density through the probe tip-sample nanogap. For an STM tip, this reflects the size and shape of the region from which electrons tunnel to the sample surface. If this area is larger than expected or desired, it may indicate problems with tip function or tip wear. This information is critical for evaluating the performance and accuracy of the STM tip and can help diagnose problems and optimize its function.

Keywords: scanning probe microscopy, field emission characteristics, probe coating, STM tungsten-graphite probes, Akiyama-gold cathodes

1 Introduction

Scanning probe microscopy is an atomic scale set of techniques used to measure and study the topography of a material surface and its properties. It started in 1982 with the invention of *Scanning Tunneling Microscopy* (STM) by Binnig *et al* [1]. STM is a vacuum tunneling technique that uses a good conductive metallic sharp tip (tungsten, platinum/iridium, iridium, …) to scan the topography of a conductive sample surface [1-4]. The tip is brought to ~ 1 nm close to the sample surface reducing the potential energy barrier between the tip and the sample surface. This enables the electrons to tunnel through the reduced potential energy barrier forming a tunneling current in the vacuum nano gap separating the tip apex and the sample [5, 6]. Although STM is a unique technique, it has several serious limitations such as the good conductivity of the sample and the scanning probe, the need for an ultra-high vacuum environment to reduce the adsorbates ratio on the scanned surface, and the limited possibility of avoiding the atomic forces that appear in the nanogap scale [7-10].

The atomic forces formed a serious challenge to STM because the STM setup does not include any parts to measure or deal with these forces. However, in 1986 Binnig made use of these forces by measuring their effects using a piezoelectric setup that includes a spring. This helped to scan the surface topography by analyzing the atomic forces and the invention of the *Atomic Force Microscopy* (AFM) [11].

In AFM, it is necessary to bring the scanning tip (which can be produced by several types of semiconducting materials) to very short distances that allow sensing of the atomic forces between the tip atoms and the sample surface atoms. Unlike STM, in AFM mode the surface topography and its properties can be studied in long (few micrometers) or short (few nanometers) separation gaps. Another useful upgrade to AFM was to produce its scanning probes from conductive materials, which is known as the conductive probe AFM (CP-AFM) technique. CP-AFM is useful for several applications such as the measurements of

[1]Institute of Scientific Instruments of the CAS, Královopolská 147, 612 00 Brno, Czech Republic
[2]Department of Microelectronics, Faculty of Electrical Engineering and Communication, Brno University of Technology, Technická 10, 616 00 Brno, Czech Republic
[3]Central European Institute of Technology, Brno University of Technology, Purkyňova 123, 612 00 Brno, Czech Republic.
[4]Department of Renewable Energy Engineering, Jadara University, Irbid 21110, Jordan
[5]Institute of Physics of Materials of the CAS, Žižkova 22, 616 00 Brno, Czech Republic
* Corresponding author: knapek@isibrno.cz

https://doi.org/10.2478/jee-2024-0033, Print (till 2015) ISSN 1335-3632, On-line ISSN 1339-309X

electrostatic forces, and the charge distribution on the sub-100 nm scale [12-17].

In all cases of SPM techniques, there is a specific part of the scanning probe tip that contributes to the measurement, and because the scanning probe is not used immediately after its fabrication, the scanning process is not believed to be done by a pure material of the probe. Instead, the measurement is performed through a layer of a native oxide of the tip material, along with adsorbed monolayers from the surrounding gases or the sample surface during the scanning process. Therefore, one of the reasons to test the tips with a thin layer of carbon is to simulate the absorption of carbon from the environment. Moreover, it is not possible to determine which part of the tip apex contributes to the measurement (although the tip apex atom has the highest probability). However, it is still possible to obtain the formal tunneling area in STM mode, or the formally affected area by the atomic force in AFM, by studying the *formal emission area* (A_f) in *field emission microscopy* (FEM). This area describes contributed tip-regen in the scanning process during an electron emission operation. It is possible to achieve this by operating the different types of scanning probes in FEM and analyzing the results by the *Forbes Field Emission Orthodoxy Testing* (FOT) [18-22].

To obtain the analysis and FOT results, Murphy-Good (MG) analysis methodology was proven in earlier work to be the best analysis methodology [20]. In MG theory, a MG-plot is a semi linear plot with the form $\ln(I.V^{-\kappa})$ vs $1/V$. The pre-exponential factor κ is the work-function related parameter that is given by $\kappa = 2 - \eta/6$, where $\eta = bc_\mathrm{S}^2\phi^{-1/2}$, where b is the universal second Fowler-Nordheim constant, c_S is the universal Schottky constant, and ϕ is the local work function of the material [20-22].

According to the MG-analysis method, the formal emission area is achieved from the slope of the MG-plot (S_MG) and its vertical axis intercept ($\ln R_\mathrm{MG}$). When these two parameters are obtained, and by defining a as the first Fowler-Nordheim universal constant, A_f is achieved according to the following equation [20-22]:

$$A_\mathrm{f} = \frac{R_\mathrm{MG}.S_\mathrm{MG}^{\kappa}}{\exp(\eta)\,.\,\eta^{\kappa-2}.a.b^2.\phi^2}$$

In this work, we study the field emission characteristics of tungsten STM nanotips, Akiyama nonconductive AFM probes, and Nenoprobe conductive AFM probes. The obtained characteristics were then analyzed using the field emission webtool described in [21–23] to obtain a good assumption for the formal active area, the effects of the native oxide or coating layers, and the effect of the aging of the probe on its performance.

2 Materials and methods

High-purity 99.99% polycrystalline tungsten wires of 0.3 mm diameter were used to prepare the STM nano tips following the electrochemical etching and cleaning techniques described in [24]. The resulting probe has a tip-apex curvature diameter of ~ 70 nm and it was coated with graphite conductive paint by dipping the tip inside graphite-isopropanol solution, which is essential to enhance the tip conductivity for ambient pressure measurements as shown in Fig. 1(a). The Akiyama nonconductive AFM probe (Nanosensors, Neuchatel, Switzerland) has a silicon tip of tip-apex curvature diameter of ~ 30 nm, and a tip height of 28 µm as presented in Fig. 1(b). Moreover, NenoProbe CP-AFM probes (Nenovision, Brno, Czech Republic) are Akiyma-like silicon-based probes coated with a layer of platinum. The tip of a NenoProbe CP-AFM has a curvature diameter of ~ 100 nm, and a tip height of ~ 10 µm as presented in Fig. 1(c).

A field emission microscope was used to obtain the field emission current-voltage characteristics described in [25]. The field emission analyses were obtained by testing the current-voltage characteristics using the field emission webtool [21-23]. Moreover, the STM and AFM measurements were obtained using the NenoVision litescope multi-functional atomic force microscope.

3 Results and discussion

3.1 Tungsten-graphite

The results obtained from the tungsten-graphite sample are presented in Fig. 2(a) for the field emission current-voltage characteristics, Fig. 2(b) for the Murphy-Good analysis plot, Fig. 2(c) for the top view of the STM scan of the Tescan calibration sample surface, and Fig. 2(d) for the bottom view of the obtained STM scan.

The current-voltage characteristics were measured until tens of nano amperes only to correlate the electron emission process in field emission mode with the electron tunneling in the scanning tunneling microscopy mode. This is because in STM the tunneling current does not exceed a few nano amperes at a vacuum gap separation distance of a few micrometers. According to Fig. 2(a), the maximum emission current achieved was ~ 35 nA, with an electrode separation distance of 1 cm, and ~ 1.46 kV of applied voltage. Following the slope (–15103 Np.V) and the vertical axis intercept (–15.998 Np) values of the MG-plot in Fig. 2(b), the results passed the orthodoxy testing providing a formal field emission area of about $A_\mathrm{f} \approx 0.4\ \mathrm{nm}^2$. Based on the A_f value, graphite coating provided an emission process with the lowest surface area contribution from a few carbon atoms, which is necessary to obtain the STM topography scans of the surface of the tested sample.

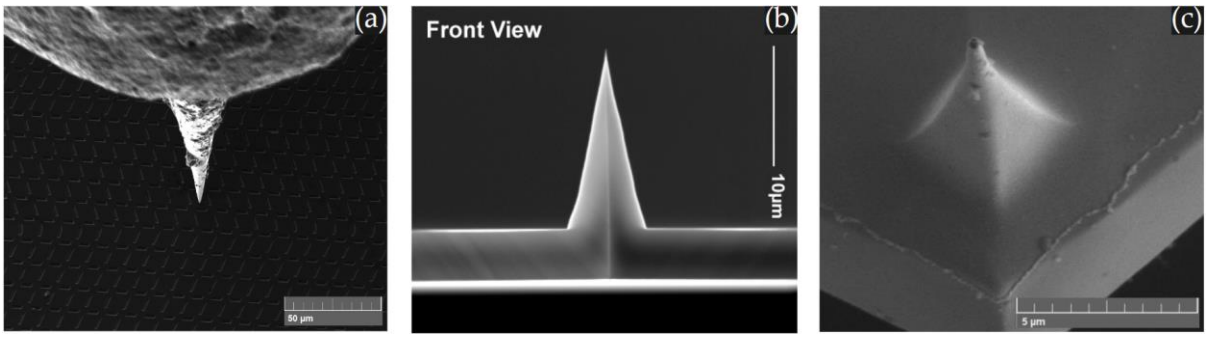

Fig. 1. Scanning electron micrographs: (a) tungsten-graphite nano tip with a scanned pattern in the background, (b) Akiyama nonconductive probe, and (c) Nenoprobe conductive probe

This information was used to measure the surface topography of a reference calibration sample in ambient pressure. The field emission analysis showed that it should be possible to obtain the STM scan without pre-cleaning of the tip surface before the scan and that the STM can be operated outside of an ultrahigh vacuum environment thanks to the presence of graphenic structure on the apex tip. This makes the tip much more conductive and thus more sensitive to fluctuations in the sample surface. The results are presented in Fig. 2(c) for the STM top view for the scanned region, and in Fig. 2(d) for the STM bottom view for the scanned region. Thus, coating tungsten tips with graphite before the STM scan helped to improve the scanning conditions for STM measurements.

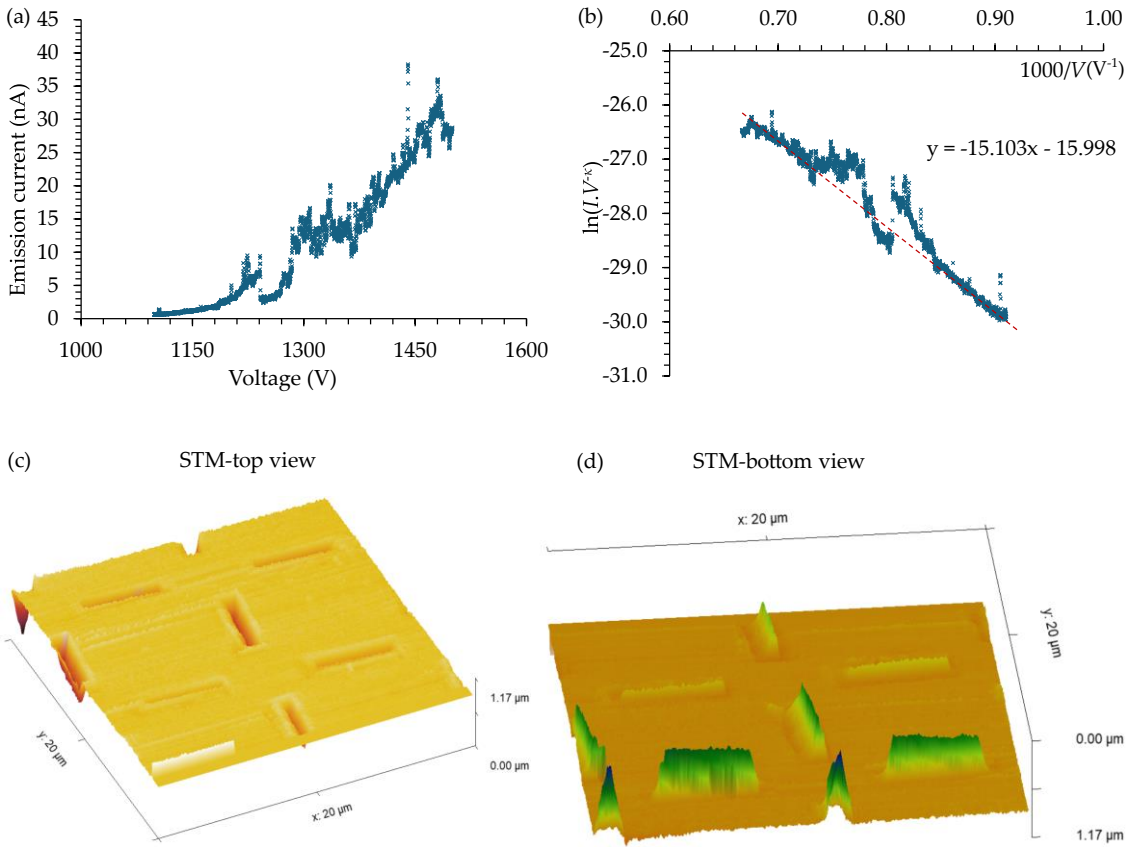

Fig. 2. Field emission (FE) and scanning tunneling microscopy (STM) results are presented: (a) by the FE current-voltage analysis, (b) FE Murphy-Good analysis plot, (c) STM top view of scanning a reference calibration sample, and (d) STM bottom view of the same scanned sample.

3.2 Akiyama-gold probe

Akiyama nonconductive probes have limited operational performance as field emission cathodes, because of the nonconductive scanning tip. However, this brought the idea of using the tip itself as a substrate to study its performance when coated with a gold nanolayer. The tip was coated with 20 nm of gold, providing 50 nm of tip diameter. The tip was tested by separating the electrodes by 0.1 mm. The current-voltage characteristics are presented in Fig. 3(a) showing high performance as a field emission cathode since the maximum emission current was ~ 1 μA, and it was achieved at a low relative applied voltage of ~ 0.8 kV. The Murphy-Good analysis plot is presented in Fig. 3(b), and it showed a more linear form than what was obtained from the tungsten-graphite sample, with a slope value of –6254.9 Np.V and vertical axis intercept value of –6.293 Np. These results are related to the better conductivity of gold when compared to graphite, and to the lower separation distance.

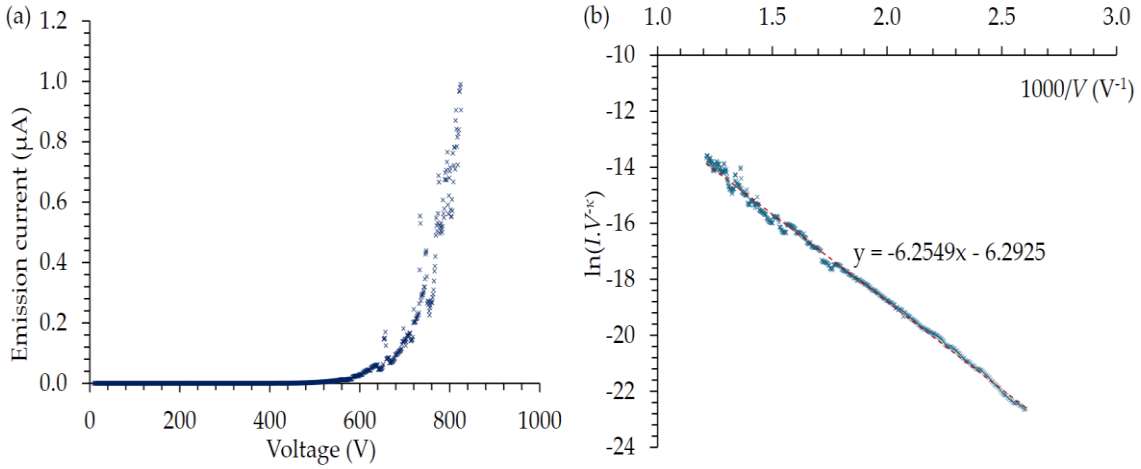

Fig. 3. Field emission (FE) results are presented: (a) by the FE current-voltage analysis, and (b) the FE Murphy-Good analysis plot as obtained from the Akiyama-gold sample.

The field emission analysis showed a good field emission performance presented by a low voltage conversion length of ~ 81.2 nm, and high contribution of the geometrical emission area with a formal emission area of $A_f \approx 40$ μm^2, which is almost equal to the whole geometrical area of a half sphere of spherical tip (39.9 μm^2) according to the half-sphere emission area model [26].

3.3 Nenoprobe conductive probe

The NenoProbe CP-AFM probes were tested similarly to the Akiyama probes with an electrodes-separation distance of 0.1 mm. Unfortunately, all the tested probes failed destructively before obtaining their current-voltage characteristics. When the applied voltage was in the range 1000 to 1500 V, it was found that the tip melted, and the connecting contacts were damaged due to a sudden surge of the emission current to high values. This may be attributed to changes in silicon conductivity (the substrate). To understand this problem, the experiment was modelled in the simulation environment COMSOL Multiphysics, version 5.4, which is a simulation software based on the finite element method.

The set-up for modelling is illustrated in Fig. 4(a). This problem deals with a silicon substrate that has a conductivity of $\sigma_{Si,0}$ =20 to 33 S/m as specified by the supplier. However, conductivity is temperature dependent. When current flows through the cathode, the electrical resistance causes the cathode to heat up by Joule heating. As the cathode heats up, the resistivity (and electrical conductivity) changes, leading to a further change in the electrical potential in the cathode region and in the vacuum region. Because these values were interdependent, we had to find a function that described the dependence of the electrical conductivity on the temperature of the n-doped silicon used to obtain a correct simulation.

To obtain the values of the concentration of donors $N_{d,}$ independent of temperature (thus we cannot calculate them through $\sigma = e\mu_n N_d$, where σ is conductivity, e is the elementary charge, since μ_n mobility depends on temperature), we used an equation from the COMSOL Multiphysics 5.4 database for n-doped silicon:

$$\sigma_{Si} = N_d e \frac{0.14}{\sqrt{1 + \frac{N_d}{\frac{N_d}{350} + 3.10^{22}}}}$$

To get the conductivity σ in S/m, N_d must be entered in m^{-3}.

Since we also need the value of N_a, which is not important for the calculation, we estimate it as $N_a = 10^{13}$ cm^{-3}. From this equation, we have obtained that N_d =0.89 to 1.34×10^{15} cm^{-3} for $\sigma_{Si,0}$ =20 to 30 S/m. The calculation of the dependence of σ_{Si} on temperature was provided from [27]. The calculation is based on the charge neutrality condition, from which the Fermi energy (E_F) is calculated. The resulting graph of the dependence on temperature is illustrated in Fig. 4(b).

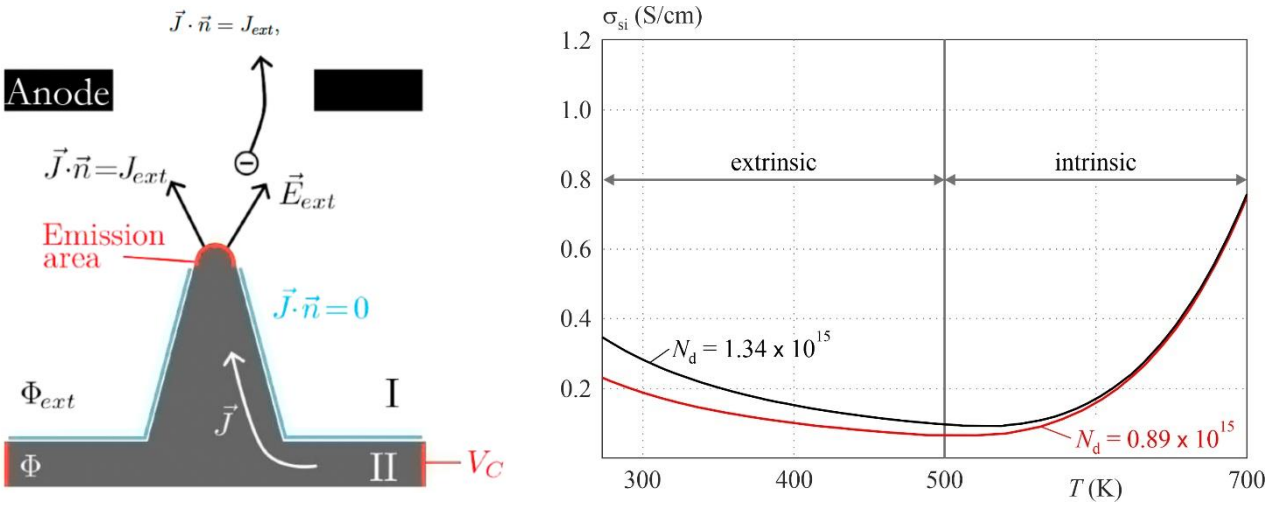

Fig. 4. The left figure explains the physics of emission from the cathode. Three different environments are defined: vacuum (I), cathode (II), and anode. Dependence of the electric conductivity σ$_{Si}$ of the n-doped silicon on temperature T, while the concentration of donors is N_d= 0.89 to 1.34×10^{15} cm^{-3} and acceptors N_a=10^{13} cm^{-3} is shown in the right figure [27].

From the following simulations, we found that at a voltage of 1300 V on the cathode, for diameter d=100 nm, distance from anode h=100 μm and conductivity of 30 S/m, the current and temperature go to infinity. As indicated above and in Fig. 4, as the temperature rises, both the electric current and conductivity increase, and since these values mutually reinforce each other, the simulation loops, causing these values to diverge indefinitely. We therefore assert that the cathode is destroyed by melting due to electron emission, with the heating occurring not gradually, but suddenly in a brief instant. The critical values, from which the destruction due to a sudden increase in conductivity is irreversible, are approximately 20 μA and 550 K. Since the jump occurs very fast, in the order of milliseconds, it is not possible to measure it on FEM. Explosive electron emission is discussed, for example, here [28]. The quasi-steady-state phase transition of the condensed cathode material into dense plasma leads to the emission of a powerful stream of electrons into vacuum. Once localized explosive electron emission events begin, the emission quickly spreads across the cathode surface as the plasma disperses. This process sustains the emission and involves additional surface areas, contributing to the abrupt increase in current. The explosion of an emission site on the surface consistently produces a liquid pool of molten material. The presence of this liquid is a critical factor in the underlying mechanisms of explosive emission. A key characteristic of this phenomenon is its exceptionally high intensity, surpassing traditional emission types by several orders of magnitude. The highest recorded current density during explosive electron emission reaches up to 10^8 A/cm² [28]. These problems were not observed with Akiyama cathodes, where the tip diameter was only ~ 12 nm, so emission could start at lower voltage values, and the higher conductivity of 40-100 S/m contributed to less Joule heating of the tip and thus a slower rise in conductivity.

4 Conclusion

In this study, we conducted a series of analyses of the surface layer functionality in different types of scanning probe microscopy (SPM) probes, focusing on the effects of coating on their emission characteristics. The three types of probes analyzed were tungsten STM probes coated with graphite, Akiyama non-conductive AFM probes coated with gold, and NenoProbe conductive AFM probes with a platinum coating. Our findings highlight the significant impact of surface coatings on their field emission properties, which are critical for their performance in SPM applications.

The coated tungsten STM probes demonstrated enhanced field emission characteristics as a result of the graphite coating. The coating minimized the contribution of the surface area to the emission process, facilitating a more precise STM scan even under ambient pressure conditions without pre-cleaning. This improvement can be attributed to the stable and conductive nature of the graphite layer, which effectively reduced the potential energy barrier for electron tunneling, thereby ensuring more accurate topography measurements.

The Akiyama non-conductive AFM probes, when coated with a gold nanolayer, exhibited substantial enhancement in field emission performance. The gold coating improved the conductivity of the probe, allowing higher emission currents at lower voltages. This enhancement is crucial for applications requiring precise electrostatic force measurements and charge distribution analysis. The gold-coated tips also displayed a more linear Murphy-Good analysis, indicating a stable and efficient emission process, further validating the effectiveness of gold as a coating material for improving probe performance.

Conversely, the NenoProbe conductive AFM probes with platinum coating encountered significant challenges. The probes experienced catastrophic failure due to sudden current surges and the resultant Joule heating, which led to the melting of the tip. This issue underscores the importance of understanding the thermal and electrical properties of the materials used in probe fabrication. The simulations revealed that the silicon substrate's conductivity increased with temperature, causing a feedback loop that led to destructive overheating. This phenomenon highlights the need for careful consideration of material properties and operational parameters to prevent such failures in future probe designs.

In conclusion, this study emphasizes the critical role of surface coatings and material properties in determining the field emission characteristics and overall performance of SPM probes. Despite being the simplest type of electron microscope, the field emission microscope (FEM) proves itself to be an invaluable tool for analyzing these characteristics. The FEM's ability to provide detailed current-voltage measurements and field emission parameters makes it an essential instrument in our study. By continuing to leverage the capabilities of FEM and other advanced microscopy techniques, researchers can further optimize SPM probes for a wide range of applications in nanotechnology, materials science, and beyond. Future research should focus on exploring alternative coating materials and advanced fabrication techniques to further improve the durability and functionality of SPM probes in various environmental conditions.

Acknowledgements

The described research was supported by the Czech Technology Agency (FW03010504) within the infrastructure provided by the Czech Academy of Sciences (RVO:68081731). The research described in the article was also financially supported by the Internal Grant Agency of the Brno University of Technology, grant number CEITEC VUT/FEKT-J-24-8567.

References

[1] G. Binnig, H. Rohrer, C. Gerber, and E. Weibel. “Surface studies by scanning tunneling microscopy”. Phys. Rev. Lett. 49, 57–61, 1982.

[2] G. Binning, and H. Rohrer, “Scanning tunneling microscopy”. Surf. Sci. 126, 236–244, 1983.

[3] G. Binnig, and H. Rohrer. “Scanning Tunneling Microscopy – From Birth to Adolescence”. Rev. Mod. Phys. 59, 615−625, 1987.

[4] C. Gerber, G. Binnig, H. Fuchs, O. Marti, and H. Rohrer. “Scanning tunneling microscope combined with a scanning electron-microscope”. Rev. Sci. Instrum. 57, 221–224, 1986.

[5] H.-J. Güntherodt R. Wiesendanger, “Scanning tunneling microscopy I”. First edition, Springer series in Surface Science, Springer-Verlag, Berlin, Germany, 1992.

[6] H.-J. Güntherodt R. Wiesendanger, “Scanning tunneling microscopy II”. First edition, Springer series in Surface Science, Springer-Verlag, Berlin, Germany, 1992.

[7] K. Besocke. “An easily operable scanning tunneling microscope”. Surf. Sci. 181, 145–153, 1987.

[8] M. Salmeron, and B. Eren, “High-Pressure Scanning Tunneling Microscopy”. Chem. Rev. 121(2), 962-1006, 2021.

[9] B. J. McIntyre, M. Salmeron, and G. A. Somorjai, “A Variable Pressure/Temperature Scanning Tunneling Microscope for SurfaceScience and Catalysis Studies”. Rev. Sci. Instrum. 64, 687−691, 1993.

[10] T. Tiedje, J. Varon, H. Deckman, and J. Stokes. “Tip contamination effects in ambient pressure scanning tunneling microscopy imaging of graphite”. J. Vac. Sci. Technol. A 6(2), 372-375, 1987.

[11] K. Bian, C. Gerber, A. J. Heinrich, D. J. Müller, S. Scheuring, and Y. Jiang. “Scanning probe microscopy”. Nat. Rev. Methods Primers 1, 36, 2021.

[12] Y. Martin, C. C. Williams, and H. K. Wickramasinghe. “Atomic force microscope force mapping and profiling on a sub 100-Å scale”. J. Appl. Phys. 61, 4723–4729, 1987.

[13] Y. F. Dufrêne, T. Ando, R. Garcia, D. Alsteens, D. Martinez-Martin, A. Engel, C. Gerber, and D. J. Müller. “Imaging modes of atomic force microscopy for application in molecular and cell biology”. Nat. Nanotechnol. 12, 295–307, 2017.

[14] D. J. Müller, A. C. Dumitru, C. Lo Giudice, H. E. Gaub, P. Hinterdorfer, G. Hummer, J. J. De Yoreo, Y. F. Dufrêne, and D. Alsteens. “Atomic Force Microscopy-Based Force Spectroscopy and Multiparametric Imaging of Biomolecular and Cellular Systems”. Chem. Rev. 121(19), 11701–11725, 2021.

[15] R. García, and Rubén Pérez. "Dynamic atomic force microscopy methods". Surf. Sci. Rep. 47(6-8), 197-301, 2002.

[16] F. J. Giessibl. “Advances in atomic force microscopy”. Rev. Mod. Phys. 75, 949, 2003.

[17] L. W. Francis, P. D. Lewis, C. J. Wright, and R. S. Conlan. “Atomic force microscopy comes of age”. Biology of the Cell 102, 133-143, 2010.

[18] R. G. Forbes. “Development of a simple quantitative test for lack of field emission orthodoxy” Proc. R. Soc. Lond. A 469, 2013.

[19] R. G. Forbes. “The Murphy–Good plot: a better method of analysing field emission data”. R. Soc. Open Sci. 6, 2019.

[20] R. G. Forbes, E. O. Popov, A. G. Kolosko, and S. V. Filippov. “The pre-exponential voltage-exponent as a sensitive test parameter for field emission theories”. Roy. Soc. Open Sci. 8, 2021.

[21] M. M. Allaham, R. G. Forbes, A. Knápek, D. Sobola, D. Burda, P. Sedlák, M. S. Mousa, Interpretation of field emission current–voltage data: Background theory and detailed simulation testing of a user-friendly webtool, Mat. Tod. Comm., 31, 2022.

[22] M. M. Allaham, R. G. Forbes, A. Knapek, and M. S. Mousa. “Implementation of the orthodoxy test as a validity check on experimental field emission data”. J. Electr. Eng. 71 (1), 37–42, 2020.

[23] M. M. Allaham, A. Knápek, M. S. Mousa and R. G. Forbes. “User-friendly method for testing field electron emission data: Technical report”. 2021 34th International Vacuum Nano-electronics Conference (IVNC), Lyon, France 2021, 1-2.

[24] [24] Z. Košelová, L. Horáková, D. Burda, M. M. Allaham, A. Knápek, Z. Fohlerová. “Cleaning of tungsten tips for subsequent use as cold field emitters or STM probes”, J. Elect. Eng. 75 (1), 41–46, 2024.

[25] A. Knápek, M. M. Allaham, D. Burda, D. Sobola, M. Drozd, M. Horáček. “Explanation of the quasi-harmonic field emission behaviour observed on epoxy-coated polymer graphite cathodes”. Mat. Tod. Comm 34, 2023.

[26] E. O. Popov, S. V. Filippov, A. G. Kolosko, and A. Knápek. “Comparison of the effective parameters of single-tip tungsten emitter using Fowler–Nordheim and Murphy–Good plots”. J. Vac. Sci. Technol. B 40 (2), 2022.

[27] “Electrical conductivity of silicon.” http://lampz.tugraz.at/~hadley/psd/L4/conductivity.php (accessed Jun. 06, 2024).

[28] N. D. Arora, J. R. Hauser, and D. J. Roulston, “Electron and Hole Mobilities in Silicon as a Function of Concentration and Temperature,” *IEEE Trans. Electron Devices*, vol. 29, no. 2, pp. 292–295, 1982.

[29] G. N. Fursey, “Field emission in vacuum micro-electronics,” *Appl. Surf. Sci.*, vol. 215, no. 1–4, pp. 113–134, Jun. 2003.

Received 2 April 2024